Journal of Power Sources 513 (2021) 230519

Contents lists available at ScienceDirect

Journal of Power Sources

journal homepage: www.elsevier.com/locate/jpowsour

Data driven analysis of lithium-ion battery internal resistance towards reliable state of health prediction

Mohammad A. Hoque [a,*], Petteri Nurmi [a], Arjun Kumar [b], Samu Varjonen [a], Junehwa Song [b], Michael G. Pecht [c], Sasu Tarkoma [a]

[a] Nodes Lab, Deaprtment of Computer Science, Exactum, P.O. Box 68 (Pietari Kalmin katu 5) 00014, University of Helsinki, Finland
[b] School of Computing Korea Advanced Institute of Science and Technology (KAIST) 335 Gwahangno, Yuseong-gu, Daejeon 34141, Republic of Korea
[c] CALCE Center for Advanced Life Cycle Engineering, 1103 Engineering Lab Building, University of Maryland, College Park, MD 20742, USA

HIGHLIGHTS

- Internal resistance offers accurate early-stage health prediction for Li-Ion batteries.
- Prediction accuracy is over 95% within the first 100 cycles at room temperature.
- Demonstrated that internal resistance dynamics characterize battery homogeneity.
- Homogeneous batteries can share the same early-stage prediction models.
- Internal resistance dynamics reliably capture usage pattern and ambient temperature.

ARTICLE INFO

Keywords:
Lithium-ion battery
State of health
Battery capacity
Internal resistance
health prediction

ABSTRACT

Accurately predicting the lifetime of lithium-ion batteries in the early stage is critical for faster battery production, tuning the production line, and predictive maintenance of energy storage systems and battery-powered devices. Diverse usage patterns, variability in the devices housing the batteries, and diversity in their operating conditions pose significant challenges for this task. The contributions of this paper are three-fold. First, a public dataset is used to characterize the behavior of battery internal resistance. Internal resistance has non-linear dynamics as the battery ages, making it an excellent candidate for reliable battery health prediction during early cycles. Second, using these findings, battery health prediction models for different operating conditions are developed. The best models are more than 95% accurate in predicting battery health using the internal resistance dynamics of 100 cycles at room temperature. Thirdly, instantaneous voltage drops due to multiple pulse discharge loads are shown to be capable of characterizing battery heterogeneity in as few as five cycles. The results pave the way toward improved battery models and better efficiency within the production and use of lithium-ion batteries.

1. Introduction

Fast and accurate prediction of the lifetime of lithium-ion batteries is vital for many stakeholders. Users of battery-powered devices can understand the effect their device usage patterns have on the life expectancy of lithium-ion batteries and improve both device usage and battery maintenance [1–3]. Battery manufacturers can enhance their battery production and verify their production methods with the help of faster prediction [4]. Enabling accurate prediction, however, is highly challenging as heterogeneity in battery production processes [5], hardware components of complex devices [6], diversity in usage patterns [6], variations in device operating conditions [7], and other factors make it difficult to model how and when the batteries are degrading accurately. In addition, due to the long life cycle of lithium-ion batteries, there is limited performance data available for building and validating prediction models.

Battery lifetime is traditionally estimated using physical models that estimate capacity loss using factors, such as the growth of the solid-electrolyte interface on battery anode [8,9], the loss of active materials [10,11], lithium plating [12,13], or impedance increase [14]. These approaches are successful in prediction, however, the chemical factors are subject to variations due to production heterogeneity, operating conditions, and usage patterns. Thus, translating the models into devices that are actively used is challenging. Another possibility is to

* Corresponding author.Nodes Lab, Deaprtment of Computer Science, Exactum, P.O. Box 68 (Pietari Kalmin katu 5) 00014.,
E-mail address: mohammad.a.hoque@helsinki.fi (M.A. Hoque).

https://doi.org/10.1016/j.jpowsour.2021.230519
Received 30 June 2021; Received in revised form 21 August 2021; Accepted 11 September 2021
Available online 1 October 2021

create models using battery voltage curves captured during charging or discharging. For example, discharge voltage curves correlate with battery health degradation [15–17]. Differential voltage curves also have been used for understanding battery health degradation [18,19] and for predicting remaining capacity [20]. These approaches depend on suitable battery instrumentation and specific cycling configurations. Similarly, voltage curves constructed during charging can be used to assess battery health [21–23]. Alternative feature representations are also possible, e.g., Lu et al. [24] modeled battery degradation as a function of four geometrical features of the charging voltage curve. Generally, these approaches have limited generality, and their performance is heavily reliant on the charging algorithm [25].

Data-driven approaches for battery lifetime modeling have recently gained traction. Since rechargeable lithium-ion batteries have a long usage time, gathering adequate data on battery health is time-consuming. The example approaches rely on various machine learning techniques, such as support vector machine [26], particle filtering [27], Bayesian predictive modeling [28], deep learning [29] and Gaussian process regression [30]. These solutions require sufficient amounts of data, and in most cases, the collected data covers over 25% of battery life degradation. These models are not for early-stage prediction as they rely on features that are difficult to estimate in practical use and require a large dataset to reach high accuracy. Indeed, the lack of sufficient data is a significant challenge for early-stage battery life prediction. Severson et al. [31] analyzed battery discharge voltage curves from the cycling information of 124 lithium-ion batteries. The authors extracted numerous statistical features from the voltage curves and developed early-stage battery life prediction models for fast charging. The features extracted during the first five cycles were also used to classify batteries as *low* and *high*-lifetime batteries. This approach relies on specialized measurements and statistical features that are difficult to estimate during the operation of a device.

This paper contributes by presenting a data-driven analysis of battery internal resistance using a comprehensive publicly available dataset of lithium cobalt oxide (LCO) batteries [32,33]. This analysis is applied to create improved early-stage battery lifetime prediction and battery characterization methods that are general and able to operate without complex instrumentation of the battery. First, it is demonstrated that battery internal resistance reliably captures various aspects of battery cycling, such as discharge current, operating condition (temperature), and the battery usage pattern in cycling. Second, based on these findings, early-stage battery health prediction models are constructed. The resistance behavior at room temperature enables predicting battery capacity with more than 95% accuracy in 100 cycles. The models for higher cycles can be used to predict the capacity of other batteries with similar accuracy, given that their internal resistance characteristics and operating conditions are identical. Finally, such features of batteries can be identified using voltage drop due to internal resistance, which also determines the heterogeneity among the cells of the similar model during the very early stage of cycling, e.g., *five* cycles. This paper overcomes the challenge of limited data points by capturing aging as a function of many pulse discharges in a cycle. Together, these contributions pave the way toward more accurate battery health predictions that can operate robustly across different lithium-ion battery chemistries, usage patterns, and working conditions.

The rest of the article is organized as follows. Section 2 provides an overview of lithium-ion battery internal resistance. The dataset is explained in Section 3. The internal resistance behavior for different cycling conditions is analyzed in Section 4 to understand the dynamics as battery health degrades with cycling. Section 5 constructs the prediction models and evaluates their performance. It also demonstrates how to characterize lithium-ion batteries according to the internal resistance dynamics. Finally, we discuss the generality of the approach and future work in Section 6. The paper concludes in Section 7.

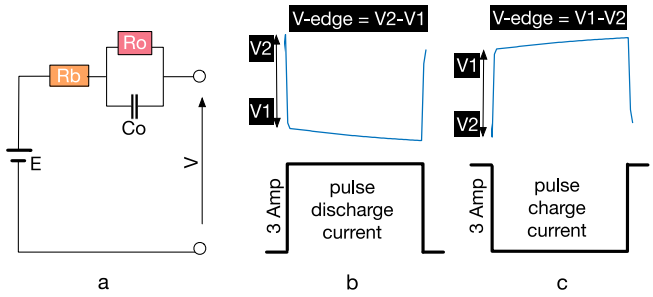

Fig. 1. (a) Thevenin battery model, (b) voltage drops for a discharge load, and (c) V-edge, i.e., voltage drop across the internal resistance R_b.

2. Background

This section first describes how to estimate the internal resistance of lithium-ion batteries from the voltage patterns due to pulsed charge and discharge currents. Next, the behavior of battery internal resistance for discharging currents, different operating temperatures, and state of charge (SoC) are discussed.

2.1. Measuring battery internal resistance

Fig. 1 illustrates battery voltage across the battery's internal resistance for a pulsed discharge/charging current of 3 A for an equivalent battery model (Thévenin model). For a discharge current I, there is a sharp drop in the battery voltage as soon as the load begins. The reason for this behavior is the battery's internal resistance R_b. This sharp change in the voltage is referred to as the V-edge value V_{edge}. Formally,

$$V_{edge} = R_b \times \Delta I = R_b \times I - R_b \times I_0, \quad (1)$$

where I_0 is the baseline current load, e.g., when the device is in sleep mode but draws some current from the battery. After the sharp drop, the battery voltage decreases almost linearly as long as the load continues. This linearity is due to the battery's double-layer capacitance (C_o), and the polarization resistance (R_o) [34]. The length of the linearity depends on the duration of the discharge load. The internal resistance due to a charging current in Fig. 1(c) can be expressed using the same equation.

2.2. Charging/discharging current

The internal resistance also depends on the amount of charging or discharging current applied to a battery in a pulse. Fig. 2 (Left) shows that voltage drop across battery internal resistance increases linearly with the pulse discharging loads for a battery. However, the resistance is inversely proportional to the applied current. Therefore, the resistance decreases exponentially as the pulse current increases (Right). These plots are constructed using a dataset [32], which is described in the next section.

2.3. Battery internal resistance and SoC

Battery internal resistance also changes as SoC changes. For example, Chen et al. [35] showed that the internal resistance is higher when a battery is fully charged or discharged. Such a pattern is consistent for different pulse discharge loads.

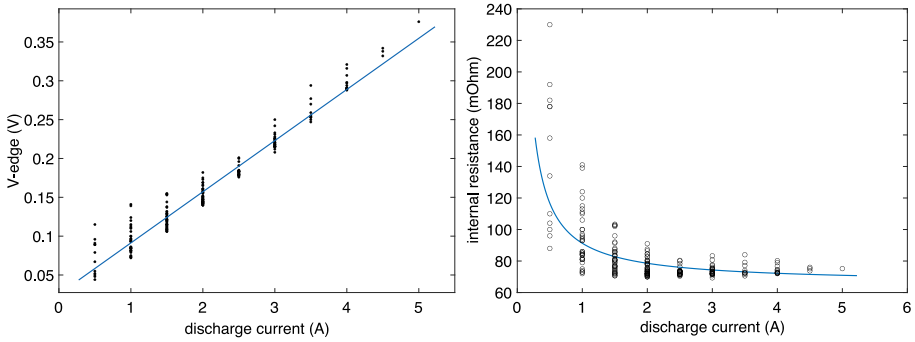

Fig. 2. (Left) V-edge Vs. discharge pulse current, (Right) battery internal resistance vs. discharge pulse current.

Table 1
Four discharge profiles and corresponding 16 batteries in the dataset.

Discharge Profile	Room temperature	40 °C
Low Current Skew	**LoCus-RT**	**LoCus-40C**
battery-id	13,14,15,16	21,22,23,24
RW Cycles	1110,1119,1124,897	511,531,505,523
Reference Cycles	22,22,22,18	11,12,11,11
RW discharge events	21510,22426,26606,20049	20170,19468,19102,20629
High Current Skew	**HiCus-RT**	**HiCus-40C**
battery-id	17,18,19,20	25,26,27,28
RW Cycles	1307,1384,1343,1284	664,605,611,613
Reference Cycles	26,27,27,26	13,12,12,12
RW discharge events	15245,12739,13705,12739	11022,9755,7447,9452

Table 2
Distribution of discharge events for different discharge load currents.

Low Skew (LS)		High Skew (HS)	
0.5A	7.2%	0.5A	2.0%
1.0A	14.8%	1.0A	2.4%
1.5A	19.3%	1.5A	3.6%
2.0A	21.6%	2.0A	6.0%
2.5A	14.6%	2.5A	9.2%
3.0A	10.0%	3.0A	11.8%
3.5A	6.5%	3.5A	17.2%
4.0A	4.0%	4.0A	23.4%
4.5A	1.5%	4.5A	19.4%
5.0A	0.5%	5.0A	5.0%

2.4. Battery internal resistance and temperature

The internal resistance value is the same for the same charging and discharging current and for a given temperature. However, the internal resistance behaves differently at different temperatures. It was shown that as the temperature increases to room temperature, the resistance of 26665 (LiFePO4) lithium-ion battery exponentially decreases and then increases again [35]. The relation is expressed in Eq. (2).

$$R_b = a \times T^2 + b \times T + c \tag{2}$$

3. Dataset

To analyze battery internal resistance and to construct prediction models for battery lifetime prediction, a publicly available lithium-ion battery dataset [32,33] is used. The dataset contains the cycling information of 24 lithium cobalt oxide (LCO) 18650 batteries of 2.2 Ah initial/design capacity. This paper considers a subset of 16 batteries cycled with a 1 min discharge pulse of different currents. The reason for excluding the remaining 8 batteries is that they had five minutes of discharge pulses. Hence, the models constructed from these measurements would not be directly comparable to the other batteries.

3.1. Battery cycling

Table 1 shows the cycling configuration of 16 batteries. A Random Walk (RW) cycle on a battery is a sequence of random discharge current loads followed by resting or idle events. The duration of each discharge event is one minute. In an idle event, the battery is neither charged nor discharged. The duration of an idle event is only a few milliseconds. The discharge loads in a cycle follow the distributions presented in Table 2. Battery voltage, temperature, and discharge currents were sampled at 1 Hz during the discharge events.

Table 1 also shows the number of such discharge events and the corresponding RW cycles per battery, which vary according to the usage or discharge profiles. Eight batteries were cycled according to low current skew distribution (**LoCus**); another eight were cycled according to a high current skew distribution (**HiCus**) as presented in Table 2. The experiments were conducted at two operating temperatures: room temperature and 40 °C. Consequently, there are four cycling profiles, as shown in Table 1.

3.2. Ground truth for battery health

After every fifty RW cycles, a *reference discharge* was performed on the batteries in the dataset. The reference discharge differs from RW cycles, repeatedly applying a sequence of operations consisting of a 1A discharge load for 10 min and a 20 min rest period until the battery was fully discharged. The capacity in Ah is computed by integrating the discharge current with time for a reference discharge sequence. These values serve as ground truth on battery health for evaluating prediction models. Since there are only a few reference cycles (Table 1), the capacity loss for individual RW cycles is estimated from the reference cycles using linear regression models. The fits of the resulting models consistently have R^2 values higher than 95%. The model coefficients are later used to estimate the State-of-Charge (SoC) and to construct new battery health prediction models in the following sections. Note that a non-linear model provides a similar fit for the data points [30], and we use the simpler model following the parsimony principle.

3.3. Extracting V-edges

A discharge current from the distribution (Table 2) is applied for one minute at a time. A sampling frequency of 1 Hz results in a voltage sequence Vd_i: $\{Vd_1, Vd_2, ..., Vd_{60}\}$, in chronological order. The discharge events are separated by a few milliseconds of a rest event of two samples Vr_i: $\{Vr_1, Vr_2\}$. Fig. 1(c) demonstrates how to compute V-edge for a discharge load, and a V-edge is computed as $(Vr_2 - Vd_1)$, where Vr_2 is the rest voltage before the discharge load is introduced. The battery internal resistance, R_b, for the events can be computed using Eq. (1) given that the idle load, I_0, is zero.

After computing the discharge current specific R_b, we separate R_bs according to SoC. As the dataset does not contain actual measurement

Table 3
Correlation between battery internal resistance (R_b) and capacity at 100th cycle for a representative battery in each profile for different SoC levels.

Discharge profile	1.0A	1.5A	2.0A	2.5A
LoCus-RT(20%)	−0.91	−0.94	−0.88	−0.94
LoCus-RT(50%)	−0.93	−0.92	−0.91	−0.90
LoCus-RT(80%)	−0.91	−0.94	−0.92	−0.90
LoCus-40C(20%)	0.55	0.6	0.62	0.63
LoCus-40C(50%)	0.54	0.60	0.63	0.64
LoCus-40C(80%)	0.53	0.61	0.63	0.65
Discharge profile	**3.0A**	**3.5A**	**4.0A**	**4.5A**
HiCus-RT(20%)	−0.85	−0.85	−0.92	−0.86
HiCus-RT(50%)	−0.88	−0.86	−0.89	−0.85
HiCus-RT(80%)	−0.87	−0.83	−0.93	−0.87
HiCus-40C(20%)	0.65	0.65	0.60	0.70
HiCus-40C(50%)	0.63	0.63	0.62	0.69
HiCus-40C(80%)	0.61	0.65	0.63	0.72

of SoC, the number of measurements, duration, discharging current, and the estimated capacity values are used to determine 20%, 50%, and 80% SoC.

4. Internal resistance dynamics and predicting battery capacity

In this section, the internal resistance dynamics of batteries are analyzed. It is shown that internal resistance dynamics capture battery health degradation due to cycling and are resilient to operating conditions. Motivated by these results, novel battery capacity prediction models are developed and evaluated.

4.1. Validity of internal resistance dynamics

This section demonstrates that internal resistance indeed captures battery aging in the early stage due to cycling. This is accomplished by computing the Pearson correlation ρ (Eq. (3)) between internal resistance (X) and battery capacity (Y) for different SoC levels. Table 3 shows statistically significant, negative correlations between internal resistance and battery capacity when the batteries are discharged at room temperature. Such correlation implies that the internal resistance of batteries increases as the capacity degrades. The strong negative correlations suggest that internal resistance is an excellent candidate feature for battery health estimation.

$$\rho = \frac{N\sum(XY) - \left(\sum(X)\sum(Y)\right)}{\sqrt{\left(N\sum X^2 - \left(\sum X\right)^2\right)\left(N\sum Y^2 - \left(\sum Y\right)^2\right)}} \tag{3}$$

At 40 °C, the relationship in Table 3 is less obvious. This is due to both temperature and discharge affecting the internal resistance. To better understand the effects of temperature, the correlations ρ for all the discharge profiles are further investigated. Fig. 3 shows that ρ is strongly positive at the beginning but steadily decreases through active usage and time. After 150 − 250 cycles, the magnitude of the correlation becomes zero, and from this point onward, the correlation ρ becomes increasingly negative and approaches −1. Previous studies have identified that such decreasing internal resistance originates from anode due to cycling [36]. In other words, the resistance of anode decreases. For this reason, initially the effect of temperature subsumes the effect of discharge on cycling [37,38]. These correlation trends and operating temperature can be the indicators for constructing accurate prediction models, as demonstrated in the next section.

4.2. Prediction model development

Internal resistance behavior is modeled as a function of battery capacity degradation for a particular discharge load and operating temperature. In the analysis, the models are constructed separately for the two operating temperatures (see Table 1). Nevertheless, the correlation trends presented in Fig. 3 hint about the operating conditions during the early phase of cycling.

Both linear and non-linear models are investigated in this section to analyze the internal resistance behavior as the battery capacity degrades through usage cycles. The intuition is that battery characteristics and operating conditions determine the best fitting model type, and thus different kinds of models are needed. To this end, battery-specific models are developed according to the profile and discharge loads rather than combining data from multiple batteries. Although some previous studies have combined data from various batteries [4,30], later in Section 5.3 it is demonstrated that the internal resistance of similar new batteries can be different, which can affect the prediction accuracy.

Linear Models: Linear prediction models are investigated as the simplest potential models. Such models are easy to integrate even with low-end battery-powered devices as the required computations are efficient and straightforward. The linear model fits a function $y = x\beta + b$, where y is the internal resistance value, β is the feature vector representing the relationship between variables, and x holds the training data points for battery capacity. However, in the early stage of cycling, a small fraction of observation data points are available. Therefore the model may struggle to learn the correct relationship between internal resistance and battery capacity.

The relationship between variables β and internal resistances y can be estimated using standard least-squares fitting of the regression lines by taking minimum from the sum of squares of the vertical deviation of the regression line from each data point. Therefore, a β is required that minimizes squared loss, i.e., $\sum_{i=1}^{n} \epsilon_i^2$. That is

$$\hat{\beta} = \arg\min_{\beta} \sum_{i=1}^{n} \epsilon_i^2 = \arg\min_{\beta} \sum_{i=1}^{n} (x_i\beta + b - y_i)^2, \tag{4}$$

where the arg min function aims to find the coefficient values that minimizes the argument.

Non-Linear Models: As for the second class, non-linear power models are considered. This is because battery capacity degradation is non-linear [7,39]. The power model is formulated as

$$y = ax^b + c. \tag{5}$$

The parameters a, b, and c can be solved by applying a logarithmic transformation on the first-order component, which results in a linear model where the parameters a and b can be estimated. This model can be substituted for the original equation to obtain a linear equation.

$$y = az + c, \tag{6}$$

where $z_i = x_i^b$. Therefore, if b is given, the values of a and c can be computed. Similarly to the sum of square in Eq. (4), the value of b can be obtained by minimizing the sum of squared loss, i.e.,

$$\hat{b} = \arg\min_{b} \sum_{i=1}^{n} (az_i + c - y_i)^2, \tag{7}$$

Next, y can be predicted by selecting the values of a and c for the b with the smallest loss and using Eq. (5).

Model Goodness: While the least square method finds the best fitting coefficients, it does not tell how good the model is in explaining the data. Therefore, the models are complemented using R^2 to measure the goodness of model fit. The R^2 values are between 0 and 1. The closer the value to 1, the better the model is predicting battery health. R^2 is computed as

$$R^2 = 1 - \frac{SS_{resid}}{SS_{total}} = 1 - \frac{\sum_{i=1}^{n}(y_i - \hat{y}_i)^2}{\sum_{i=1}^{n}(y_i - \bar{y}_i)^2}, \tag{8}$$

where SS_{resid} sum of square of the residuals from the regression, and SS_{total} is the sum of the squared differences of the response variable from the mean.

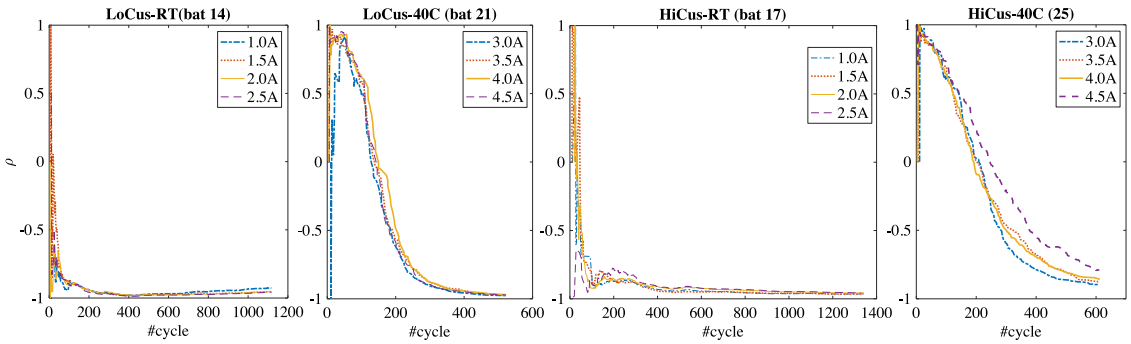

Fig. 3. Pearson correlation trend between battery internal resistance (R_b) and battery capacity as the batteries are discharged within 80% SoC level. At room temperature, the correlation becomes strongly negative within the first 100 cycle. At 40 °C, the correlation gradually proceeds towards negative.

Evaluation Metrics: The evaluation assesses the prediction performance of our models using standard error measures for regression. Specifically, the Root Mean Square Error (RMSE) and the median percentage error (MPAE) are considered to evaluate the models' performance. RMSE is defined as

$$RMSE = \sqrt{\frac{\sum_{i=1}^{n}(y_i - \hat{y}_i)^2}{n}} \tag{9}$$

and (MAPE):

$$\%error = \sum_{i=1}^{n} \frac{|y_i - \hat{y}_i|}{y_i} \times 100. \tag{10}$$

4.3. Fit of the prediction models

This section examines the prediction models to explain how internal resistance changes as battery capacity reduces using the metrics presented in the earlier section. Fig. 4 illustrates the fitted regression models of internal resistance values against the battery capacity at room temperature. The presented coefficients are shown with 95% confidence bounds. The model fits in all cases are above 0.95, irrespective of the discharge loads and the discharge profiles. The figure also shows that the internal resistance behavior follows the second-order power function as the capacity reduces due to cycling. However, the behavior of internal resistance differs significantly according to the discharge load. Consequently, the coefficients also vary among similar profiles as shown in Fig. 4(c) & (d). We observed similar patterns with all the batteries of **LoCus-RT** and **HiCus-RT** profiles presented in Table 1.

In contrast, Fig. 5 depicts the behavior of internal resistance when the batteries are cycled at 40 °C. Similar to the correlation patterns shown in Section 4.1, the figure shows that internal resistance initially decreases sharply from a higher value and then gradually increases. Meanwhile, the batteries lose a small fraction of the initial capacity. The pattern follows the second-order exponential function, further explaining the variations in correlation patterns shown in Fig. 3. Such a pattern is consistent across multiple discharge loads, profile variation presented in Fig. 5, and across other batteries with similar profiles presented in Table 1. The only exception was battery 26. We believe that there were some measurement anomalies as the dynamics do not follow the models discussed earlier.

Fig. 5 also shows that a linear model can have a very good fit by skipping early-stage usage data where the effect of temperature dominates the effect of discharge. The batteries with **LoCus-40C** profile can have fitness as good as 0.95 once the early-stage data is skipped. For **HiCus-40C** batteries, model goodness slightly deteriorates due to more sparse measurements than room temperature. However, even in this case the overall fit is excellent, consistently being above 0.85 (Fig. 5(c) & (d)).

To examine whether other types of models better explain the relationship between internal resistance and capacity, a linear regression model is also investigated for the **LoCus-RT** and **HiCus-RT** profiles. Table 4 shows slightly poorer fits compared to the power degree model. Hence, simple linear models might be sufficient to predict battery capacity changes within a smaller cycle range. In general, the R^2 values for all profiles in Figs. 4 and 5 are approximately 0.95, which indicates that variance in internal resistance values is almost around its mean irrespective of the ambient temperature. However, the R^2 values for the **HiCus** profiles at 40 °C are slightly lower at 0.85. Thus, the results imply that the model's performance is sensitive to temperature and higher discharge rates, with a slightly decreasing model fit.

Table 4
Goodness of model fit (R^2) for four representative batteries according to usage profile and discharge load at 80% SoC.

Model	**ax+b**	**ax^b+c**	**ax+b**	**ax^b+c**
LoCus-RT	0.95(1.5A)	0.98(1.5A)	0.95(2A)	0.98(2A)
HiCus-RT	0.95(3.5A)	0.96(3.5A)	0.96(4.0A)	0.96(4.0A)
Model	**ax+b**		**ax+b**	
	0.94(1.5A)		0.91(2A)	
HiCus-40C	0.81(3.5A)		0.84(4A)	

Figs. 4 and 5 demonstrate internal resistance dynamics when the SoC is 80%. Fig. 6 shows that the pattern overlaps for 20% and 50% SoC as well for a battery. These results highlight that the battery's internal resistance dynamics are not affected by SoC. As demonstrated in Figs. 4 and 5, the dynamics of internal resistance significantly differ in room temperature and in 40 °C temperature. However, it was shown that battery internal resistance has similar values at 17 °C and 40 °C [35], though the trend is decreasing and increasing respectively as the temperature increases from 17 °C. However, we need further investigation to understand the resistance dynamics at such lower temperature.

5. Performance evaluation

This section constructs the prediction models using data from early cycles and evaluates their performance. Early-stage prediction models are essential to understand the performance of the batteries before significant capacity degradation occurs. Among others, they enable re-calibration of device load and selecting the appropriate battery technology to use. The early prediction of battery health involves predicting battery health using internal resistance (80% SoC) at the early life stage, i.e., with as few cycles as possible.

5.1. Early prediction of battery health

Although the models presented earlier may have very good fits, their performance can vary significantly when only small amounts of data are available from cycling. This section demonstrates that the internal resistance-based models have good performance even when small amounts of data are available. Data from the first 100 – 200 cycles

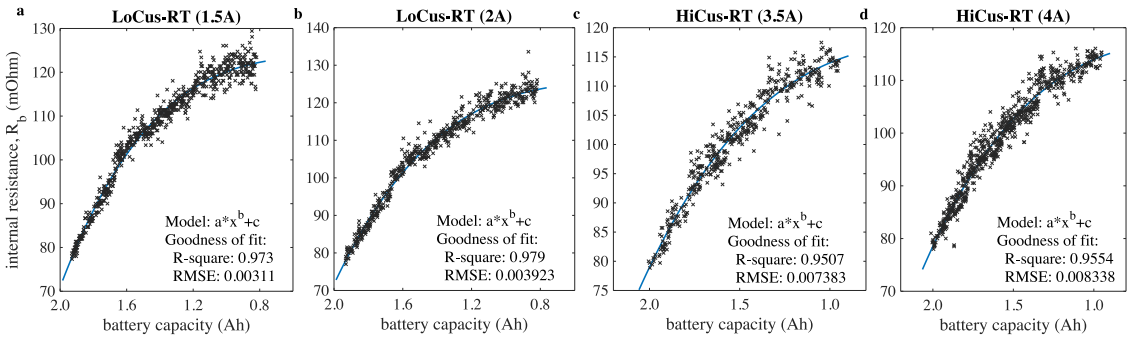

Fig. 4. The changes in internal resistance, R_b, as the capacity degrades. The internal resistance values are collected when the SoC is above 80%. Figure (a,b), Second order Power regression model captures internal resistance dynamics for the batteries with **LoCus-RT** profile. Figure (c,d), Similar Power function fits for the batteries with **HiCus-RT** profile.

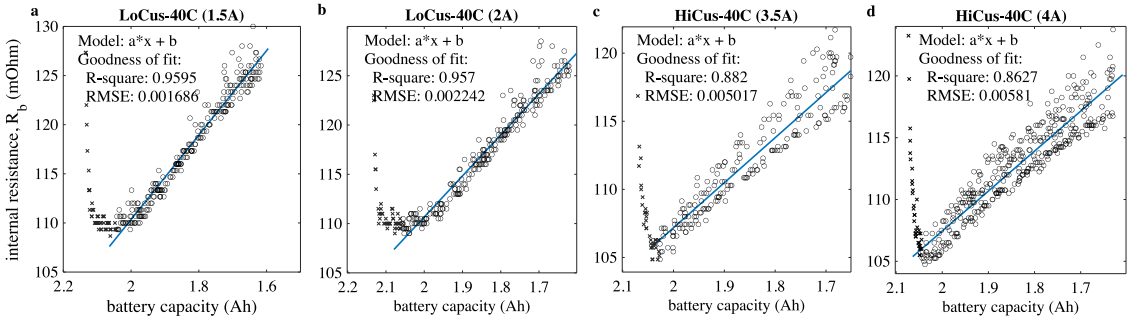

Fig. 5. The internal resistance dynamics at 80% SoC, R_b, as the battery capacity reduces due to RW cycling at 40 ° C. Figure (a,b), Linear first degree polynomial fits for the battery with **LoCus-40C** profile after 100 cycles. Figure (c,d), First degree polynomial fit for another battery with **HiCus-40C** profile after 100 cycles.

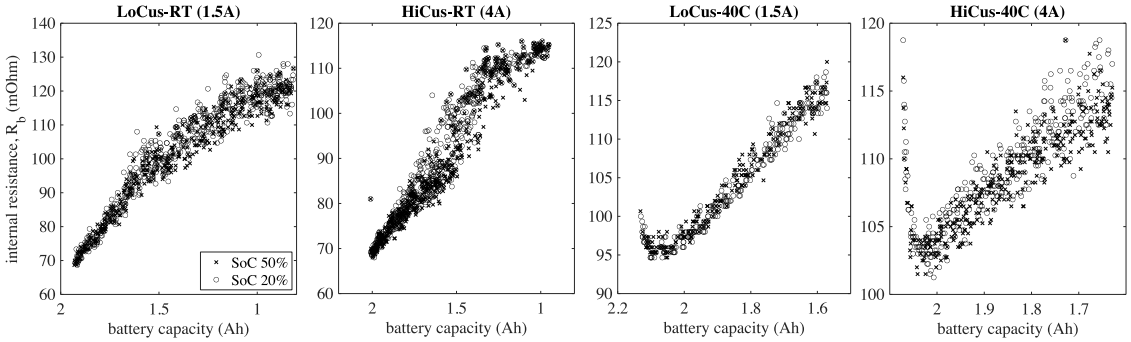

Fig. 6. Battery internal resistance dynamics when the battery state of charges are 50% and 20% respectively.

are used to construct the models. The data from successive 50–100 cycles are used to evaluate model performance.

The models are constructed by progressively increasing the cycle count until the model reaches a reasonable mean absolute percentage error (MAPE). Table 5 shows that the linear models for the batteries with **LoCus-RT** and **HiCus-RT** profiles suffer from 1%–5% error in predicting battery capacity. In other words, these room temperature models achieve more than 90% accuracy within 100 cycles.

The prediction models are excellent during the early cycles for 12 of the 16 batteries, corresponding to 3 of the 4 usage profiles. The **HiCus-40C** and **LoCus-40C** models are constructed with 100 cycles data and have 92%–99% accuracy. However, the resistance values from the first 50–100 cycles are ignored due to the exponential pattern presented in Fig. 5. The batteries of **LoCus-40C** profiles have better accuracy compared to the **HiCus-40C** models. Fig. 5 also shows that the data points are more scattered with this profile **HiCus-40C**. Thus, it is possible to construct good prediction models with internal resistance from a smaller amount of battery pulse discharge information. This may vary from battery to battery, even though they are cycled with similar usage profiles.

5.2. Transfer learning

This section assesses the transfer capability of the models and their generality. Specifically, the models are constructed from the first battery (i.e., the one with the lowest identifier in the dataset) in each category shown in Table 5 and the model for that battery is used to predict the capacity of the other three batteries. The internal resistance of the remaining batteries is not considered in constructing the models in this evaluation. Similar prediction models, demonstrated in Figs. 4 and 5, are derived from longer cycling data.

Fig. 7 demonstrates that the resulting predictions are closely aligned with the actual values. In line with the other results, the performance is best for the non-linear models constructed for batteries operating at room temperature, for which the MAPE is within 5%. In fact, the remaining six batteries of **LoCus-RT** and **HiCus-RT** profiles had MAPE less than 8%.

In contrast, only two batteries from the **LoCus-40C** & **HiCus-40C** profiles can share the linear models with other batteries with good performance. The remaining six batteries of these profiles have MAPE within 10%–20%. Such performance is expected, as the internal

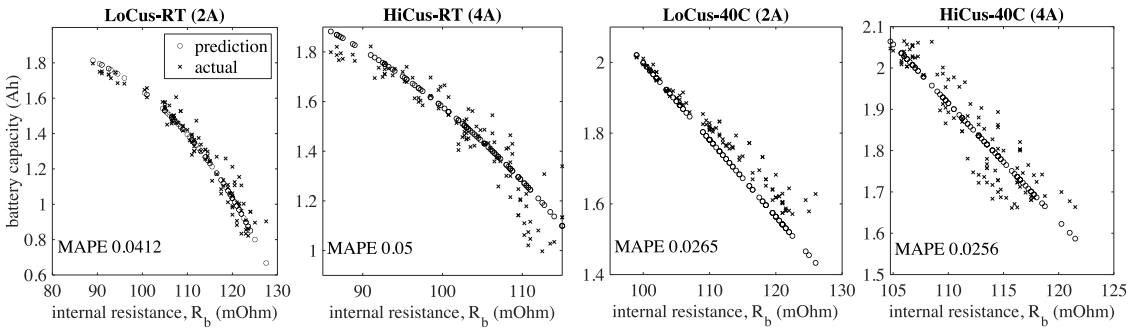

Fig. 7. Transfer learning and the performance of the regression models in Figs. 4 and 5 for the remaining batteries.

Table 5
The mean absolute percentage error (MAPE) of the linear regression models constructed from the partial active usage data of the 16 batteries (80% SoC). The room temperature models are constructed from the internal resistance of the first 100 RW cycles data, whereas the higher temperature (40 °C) models are constructed by skipping first 50–200 cycles.

LoCus-RT (2A)	**Bat-13**	**Bat-14**	**Bat-15**	**Bat-16**
Training RW Cycles	0–100	0–100	0–100	0–100
Testing RW Cycles	101–200	101–200	101–200	101–200
MAPE	0.02	0.02	0.02	0.01
LoCus-40C (2A)	**Bat-21**	**Bat-22**	**Bat-23**	**Bat-24**
Training RW Cycles	5–150	50–150	50–150	50–150
Testing RW Cycles	151–250	151–250	151–250	151–250
MAPE	0.02	0.02	0.01	0.08
HiCus-RT (4A)	**Bat-17**	**Bat-18**	**Bat-19**	**Bat-20**
Training RW Cycles	0–100	0–100	0–100	0–100
Testing RW Cycles	101–200	101–200	101–200	101–200
MAPE	0.03	0.03	0.01	0.05
HiCus-40C (4A)	**Bat-25**	**Bat-26**	**Bat-27**	**Bat-28**
Training RW Cycles	50–150	–	50–150	100–200
Testing RW Cycles	151–200	–	151–250	201–250
MAPE	0.01	–	0.01	0.01

resistance across the batteries of having the same capacity can vary, as demonstrated in Section 5.3.

However, the performance demonstrates that a model from a used battery can be applied to another new battery as long as the operating conditions are sufficiently similar—the possibility to share models increases when the batteries are used at room temperature. The variation of the internal resistance among new batteries also contributes to different prediction models, as demonstrated in the next section.

5.3. Characterizing batteries of same model

This section characterizes batteries using the V-edge values but for multiple discharge loads, as the relation is linear compared to the internal resistance (see Fig. 2). Fig. 8 shows the linear models for the 16 batteries cycled at the four different operating conditions described in Table 1. The models are constructed from the first 5 RW cycles of each battery, and the fits for all models exceed 95%.

The regression plots in Fig. 8 show that most of the batteries in the dataset have similar internal resistance models in every operating condition. Only one or two batteries in each group have coefficients that differ significantly. This indicates that the differences between the linear models can be used to separate batteries according to their internal resistance characteristics. Fig. 8 also illustrates that the resistance is particularly similar when the discharge current is low, which suggests that a single resistance value might not be sufficient to construct the necessary characterization.

6. Discussions and future work

To summarize, internal resistance-based models can accurately explain the impact of different discharge loads and temperatures on battery capacity. Best performance results under normal operating temperatures, and as the temperature or battery discharge profile changes, the performance degrades slightly. Even in this case, our models' accuracy remains consistently high, reaching over 90% from the early stage usage data. Utilizing a battery model for another battery depends on how similar the batteries are in their internal resistance. Besides, the resistance values from multiple homogeneous batteries should be used to construct more accurate prediction models. Overall, these are very encouraging results, suggesting that internal resistance is an outstanding candidate feature to predict battery health.

Table 6 compares recent data-driven health prediction approaches with this work. A recent work considered a large dataset containing the cycling information of 124 lithium-ion batteries [4]. The batteries were discharged with continuous discharge currents and charged with 72 different fast charging conditions. The authors developed the prediction models from the resulting voltage curves from many batteries during the early stage of cycling (100 cycles). Those models could predict battery health in an early stage with more than 95% accuracy but require extensive amounts of data, and the resulting features are sensitive to the way the battery is used.

Richardson et al. [30] investigated the Random Walk dataset to predict battery health. They relied on Gaussian process regression to predict battery health based on usage patterns. They considered the distributions of current, the discharge rate of stored charge, voltage, and temperature for the discharge load patterns as the input features. Their training includes data from 50% percent cells in the dataset and derived 96% accurate models. These models rely on features that are difficult to estimate in practical use, and require a large dataset to reach high accuracy.

In contrast, this paper demonstrates that the internal cell resistance is an excellent candidate feature for battery health prediction using the same dataset. Its dynamics correlate very well with battery health at the early stage of cycling, and simple models are sufficient to capture the dynamics. Internal cell resistance can be estimated from information available to the battery interface, in contrast to the models described above, which require external details on operating conditions or device usage. The best early-stage prediction models are achieved at room temperature and are more than 95% accurate. Furthermore, it is demonstrated how to separate batteries based on their internal resistance characteristics. This can be used, e.g., to select the optimal prediction model to use.

This paper has investigated LCO batteries; however, the resistance dynamics and prediction models should apply to lithium-ion batteries with different chemistries. For example, Kiel [40] presented that lithium nickel cobalt aluminum oxide (NCA) batteries exhibit nonlinear patterns at 40 °C, similar to those shown in Fig. 5. Nevertheless, the coefficients of the prediction models should vary according to the

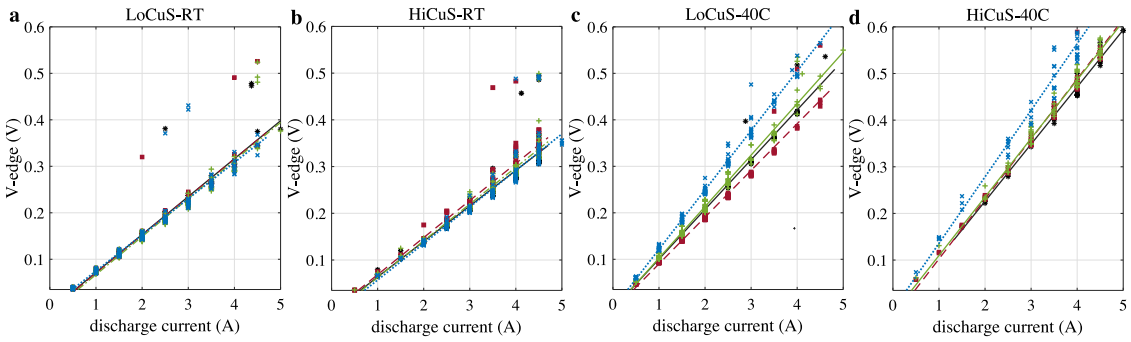

Fig. 8. The regression models for internal resistance and discharge loads for 16 batteries. The resistance values are taken from the first *5* RW cycle and the Linear Regression fits have very good fits are computed for four discharge profiles. Figure **(a, b)**, The cells have similar regression coefficients. Figure **(c,d)**, At least one of the cells has different regression coefficients.

Table 6
Comparison among the data-driven approaches for predicting battery life.

Model	Accuracy	Dataset (Cells)	Features	Early prediction	Production heterogeneity
Linear Models [4]	95%	128	Discharge Voltage Curve	Yes	Yes
Gaussian Process [30]	96%	24	Distributions of discharge Voltage, current, temperature, discharge rate of stored charge	No	No
Linear/ non-Linear Models	95%	16	Internal resistance, V-edge	Yes	Yes

usage patterns and operating conditions. They also might require more cycles to have a reasonable correlation between internal resistance and capacity degradation. The initial reduction of resistance of anode at higher temperatures is an interesting phenomenon as well. Future steps include exploring the resistance dynamics at lower and higher than room temperatures and shedding light on the initial decrease of resistance.

7. Conclusions

This paper performed a data-driven analysis of battery internal resistance and modeled the internal resistance dynamics of lithium-ion batteries. The analysis demonstrates that battery internal resistance dynamics strongly correlate with the capacity for actual usage conditions even at the early stage of cycling. Models capturing the internal resistance can predict capacity with more than 95% accuracy when the batteries are cycled with four different real-world usage profiles at room temperature and 40 °C. It is also possible to reuse those models for other batteries when the resistance dynamics and operating conditions are sufficiently similar, as demonstrated. The results offer a novel way to predict remaining battery capacity at an early stage and pave the way toward better battery management and production solutions.

CRediT authorship contribution statement

Mohammad A. Hoque: Conceptualization, Data analysis, Writing. **Petteri Nurmi:** Writing – review & editing. **Arjun Kumar:** Data Preparation, Early Draft. **Samu Varjonen:** Data Preparation, Reviewing. **Junehwa Song:** Reviewing. **Michael G. Pecht:** Reviewing, Supervision. **Sasu Tarkoma:** Review, Supervision.

Declaration of competing interest

The authors declare that they have no known competing financial interests or personal relationships that could have appeared to influence the work reported in this paper.

Acknowledgment

This research is partly supported by the Academy of Finland project CBAI (Crowdsourced Battery Optimization AI for a Connected World) grant no 1319017.

References

[1] S.B. Peterson, J. Apt, J.F. Whitacre, Lithium-ion battery cell degradation resulting from realistic vehicle and vehicle-to-grid utilization, J. Power Sources 195 (2010) http://dx.doi.org/10.1016/j.jpowsour.2009.10.010.

[2] V. Ramadesigan, Modeling and simulation of lithium-ion batteries from a systems engineering perspective, J. Electrochem. Soc. 159 (2012) http://dx.doi.org/10.1149/2.018203jes.

[3] W. Waag, C. Fleischer, D.U. Sauer, Critical review of the methods for monitoring of lithium-ion batteries in electric and hybrid vehicles, J. Power Sources 258 (2014) http://dx.doi.org/10.1016/j.jpowsour.2014.02.064.

[4] K. Severson, P. Attia, N. Jin, N. Perkins, B. Jiang, Z. Yang, M. Chen, M. Aykol, P. Herring, D. Fraggedakis, M. Bazant, S. Harris, W. Chueh, R. Braatz, Data-driven prediction of battery cycle life before capacity degradation, Nat. Energy 4 (2019) 1–9, http://dx.doi.org/10.1038/s41560-019-0356-8.

[5] T. Baumhöfer, M. Brühl, S. Rothgang, D.U. Sauer, Production caused variation in capacity aging trend and correlation to initial cell performance, J. Power Sources 247 (2014) http://dx.doi.org/10.1016/j.jpowsour.2013.08.108.

[6] S.F. Schuster, M.J. Brand, P. Berg, M. Gleissenberger, A. Jossen, Lithium-ion cell-to-cell variation during battery electric vehicle operation, J. Power Sources 297 (2015) http://dx.doi.org/10.1016/j.jpowsour.2015.08.001.

[7] S.F. Schuster, Nonlinear aging characteristics of lithium-ion cells under different operational conditions, J. Energy Storage 1 (2015) http://dx.doi.org/10.1016/j.est.2015.05.003.

[8] S. Sankarasubramanian, B. Krishnamurthy, A capacity fade model for lithium-ion batteries including diffusion and kinetics, Electrochim. Acta 70 (2012) 248–254, http://dx.doi.org/10.1016/j.electacta.2012.03.063.

[9] M.B. Pinson, M.Z. Bazant, Theory of SEI formation in rechargeable batteries: capacity fade, accelerated aging and lifetime prediction, J. Electrochem. Soc. 160 (2012) http://dx.doi.org/10.1149/2.044302jes.

[10] J. Christensen, J. Newman, Cyclable lithium and capacity loss in Li-ion cells, J. Electrochem. Soc. 152 (2005) http://dx.doi.org/10.1149/1.1870752.

[11] Q. Zhang, R.E. White, Capacity fade analysis of a lithium ion cell, J. Power Sources 179 (2008) http://dx.doi.org/10.1016/j.jpowsour.2008.01.028.

[12] D. Anseán, Operando lithium plating quantification and early detection of a commercial LiFePO4 cell cycles under dynamic driving schedule, J. Power Sources 356 (2017) http://dx.doi.org/10.1016/j.jpowsour.2017.04.072.

[13] X.G. Yang, Y. Leng, G. Zhang, S. Ge, C.Y. Wang, Modeling of lithium plating induced aging of lithium-ion batteries: transition from linear to nonlinear aging, J. Power Sources 360 (2017) http://dx.doi.org/10.1016/j.jpowsour.2017.05.110.

[14] A. Cordoba-Arenas, S. Onori, Y. Guezennec, G. Rizzoni, Capacity and power fade cycle-life model for plug-in hybrid electric vehicle lithium-ion battery cells containing blended spinel and layered-oxide positive electrodes, J. Power Sources 278 (2015) http://dx.doi.org/10.1016/j.jpowsour.2014.12.047.

[15] A. Kumar, M.A. Hoque, P. Nurmi, M.G. Pecht, S. Tarkoma, J. Song, Battery health estimation for iot devices using v-edge dynamics, in: Proceedings of the 21st International Workshop on Mobile Computing Systems and Applications, in: HotMobile '20, Association for Computing Machinery, New York, NY, USA, 2020, pp. 56–61, http://dx.doi.org/10.1145/3376897.3377858.

[16] M. Dubarry, C. Truchot, B.Y. Liaw, Synthesize battery degradation modes via a diagnostic and prognostic model, J. Power Sources 219 (2012) http://dx.doi.org/10.1016/j.jpowsour.2012.07.016.
[17] M. Berecibar, M. Garmendia, I. Gandiaga, J. Crego, I. Villarreal, State of health estimation algorithm of LiFePO4 battery packs based on differential voltage curves for battery management system application, Energy 103 (2016) http://dx.doi.org/10.1016/j.energy.2016.02.163.
[18] A.J. Smith, J.C. Burns, J.R. Dahn, High-precision differential capacity analysis of LiMn2O4/graphite cells, Electrochem. Solid-State Lett. 14 (2011) http://dx.doi.org/10.1149/1.3543569.
[19] I. Bloom, An accelerated calendar and cycle life study of Li-ion cells, J. Power Sources 101 (2001) http://dx.doi.org/10.1016/S0378-7753(01)00783-2.
[20] K. Honkura, K. Takahashi, T. Horiba, Capacity-fading prediction of lithium-ion batteries based on discharge curves analysis, J. Power Sources 196 (23) (2011) 10141–10147, http://dx.doi.org/10.1016/j.jpowsour.2011.08.020, URL https://www.sciencedirect.com/science/article/pii/S0378775311015199.
[21] M.A. Hoque, M. Siekkinen, J. Koo, S. Tarkoma, Full charge capacity and charging diagnosis of smartphone batteries, IEEE Transactions on Mobile Computing 16 (11) (2017) 3042–3055, http://dx.doi.org/10.1109/TMC.2017.2688321.
[22] Y. Zheng, C. Qin, X. Lai, X. Han, Y. Xie, A novel capacity estimation method for lithium-ion batteries using fusion estimation of charging curve sections and discrete Arrhenius aging model, Appl. Energy 251 (2019) 113327, http://dx.doi.org/10.1016/j.apenergy.2019.113327.
[23] Z. Wang, S. Zeng, J. Guo, T. Qin, Remaining capacity estimation of lithium-ion batteries based on the constant voltage charging profile, PLoS One 13 (7) (2018) e0200169.
[24] C. Lu, L. Tao, H. Fan, Li-ion battery capacity estimation: A geometrical approach, J. Power Sources 261 (2014) 141–147, http://dx.doi.org/10.1016/j.jpowsour.2014.03.058.
[25] M.A. Hoque, S. Tarkoma, Characterizing smartphone power management in the wild, in: Proceedings of the 2016 ACM International Joint Conference on Pervasive and Ubiquitous Computing: Adjunct, in: UbiComp '16, ACM, New York, NY, USA, 2016, pp. 1279–1286, http://dx.doi.org/10.1145/2968219.2968295.
[26] A. Nuhic, T. Terzimehic, T. Soczka-Guth, M. Buchholz, K. Dietmayer, Health diagnosis and remaining useful life prognostics of lithium-ion batteries using data-driven methods, J. Power Sources 239 (2013) http://dx.doi.org/10.1016/j.jpowsour.2012.11.146.
[27] C. Hu, G. Jain, P. Tamirisa, T. Gorka, Method for estimating the capacity and predicting remaining useful life of lithium-ion battery, Appl. Energy 126 (2014) http://dx.doi.org/10.1016/j.apenergy.2014.03.086.
[28] X. Hu, J. Jiang, D. Cao, B. Egardt, Battery health prognosis for electric vehicles using sample entropy and sparse Bayesian predictive modeling, IEEE Trans. Ind. Electron. 63 (2016).
[29] Y. Zhang, R. Xiong, H. He, M. Pecht, Long short-term memory recurrent neural network for remaining useful life prediction of lithium-ion batteries, IEEE Trans. Veh. Technol. 67 (2018) http://dx.doi.org/10.1109/TVT.2018.2805189.
[30] R.R. Richardson, M.A. Osborne, D.A. Howey, Battery health prediction under generalized conditions using a Gaussian process transition model, J. Energy Storage 23 (2019) 320–328, http://dx.doi.org/10.1016/j.est.2019.03.022, URL https://www.sciencedirect.com/science/article/pii/S2352152X18307734.
[31] K. Severson, P. Attia, N. Jin, N. Perkins, B. Jiang, Z. Yang, M. Chen, M. Aykol, P. Herring, D. Fraggedakis, M. Bazant, S. Harris, W. Chueh, R. Braatz, Data-driven prediction of battery cycle life before capacity degradation, Nat. Energy 4 (2019) 1–9, http://dx.doi.org/10.1038/s41560-019-0356-8.
[32] B. Bole, C. Kulkarni, M. Daigle, Randomized battery usage data set, NASA AMES Progn. Data Repos. 70 (2014).
[33] B. Bole, C. Kulkarni, M. Daigle, Adaptation of an electrochemistry-based Li-Ion battery model to account for deterioration observed under randomized use, in: PHM 2014 - Proceedings of the Annual Conference of the Prognostics and Health Management Society 2014, p. 9, 2014, https://doi.org/10.36001/phmconf.2014.v6i1.2490.
[34] A. Barai, K. Uddin, W.D. Widanage, A. McGordon, P. Jennings, A study of the influence of measurement timescale on internal resistance characterisation methodologies for lithium-ion cells, Sci. Rep. 8 (2017).
[35] Y. Chen, Y. Ma, P. Duan, H. Chen, Estimation of state of charge for lithium-ion battery considering effect of aging and temperature, in: 2018 37th Chinese Control Conference (CCC), 2018, pp. 8472–8477, https://doi.org/10.23919/ChiCC.2018.8483968.
[36] B. Stiaszny, J.C. Ziegler, E.E. Krauß, J.P. Schmidt, E. Ivers-Tiffée, Electrochemical characterization and post-mortem analysis of aged LiMn2O4–Li(Ni0.5Mn0.3Co0.2)O2/graphite lithium ion batteries. Part I: Cycle aging, J. Power Sources 251 (2014) 439–450, http://dx.doi.org/10.1016/j.jpowsour.2013.11.080, URL.
[37] A. Franco, Rechargeable Lithium Batteries: From Fundamentals To Applications, Elsevier, 2015.
[38] J. Remmlinger, M. Buchholz, M. Meiler, P. Bernreuter, K. Dietmayer, State-of-health monitoring of lithium-ion batteries in electric vehicles by on-board internal resistance estimation, J. Power Sources 196 (12) (2011) 5357–5363.
[39] S. Paul, C. Diegelmann, H. Kabza, W. Tillmetz, Analysis of ageing inhomogeneities in lithium-ion battery systems, J. Power Sources 239 (2013) http://dx.doi.org/10.1016/j.jpowsour.2013.01.068.
[40] P. Keil, Aging of lithium-ion batteries in electric vehicles, Technische Universität München, 2017.